Aging, microglia and cytoskeletal regulation are key factors in the pathological evolution of the APP23 mouse model for Alzheimer's disease

Janssen, Leen; Dubbelaar, Marissa L.; Holtman, Inge R.; de Boer-Bergsma, Jelkje; Eggen, Bart J. L.; Boddeke, Hendrikus W. G. M.; De Deyn, Peter P.; Dam, van, Debby

Published in:
Biochimica et biophysica acta-Molecular basis of disease

DOI:
10.1016/j.bbadis.2016.11.014

Publication date:
2017

Biochimica et Biophysica Acta 1863 (2017) 395–405

Contents lists available at ScienceDirect

Biochimica et Biophysica Acta

journal homepage: www.elsevier.com/locate/bbadis

Aging, microglia and cytoskeletal regulation are key factors in the pathological evolution of the APP23 mouse model for Alzheimer's disease

Leen Janssen [a], Marissa L. Dubbelaar [b], Inge R. Holtman [b], Jelkje de Boer-Bergsma [c], Bart J.L. Eggen [b], Hendrikus W.G.M. Boddeke [b], Peter P. De Deyn [a,d,e,f], Debby Van Dam [a,d,*]

[a] Laboratory of Neurochemistry and Behavior, Institute Born-Bunge, University of Antwerp, Antwerp, Belgium
[b] Department of Neuroscience, Medical Physiology Section, University of Groningen, University Medical Center Groningen (UMCG), Groningen, The Netherlands
[c] University of Groningen, University Medical Center Groningen, Department of Genetics, Groningen, The Netherlands
[d] Department of Neurology and Memory Clinic, Hospital Network Antwerp (ZNA) Middelheim and Hoge Beuken, Antwerp, Belgium
[e] University of Groningen, University Medical Center Groningen (UMCG), Department of Neurology and Alzheimer Research Center, Groningen, The Netherlands
[f] Biobank, Institute Born-Bunge, University of Antwerp, Antwerp, Belgium

ARTICLE INFO

Article history:
Received 22 June 2016
Received in revised form 21 October 2016
Accepted 8 November 2016
Available online 10 November 2016

Keywords:
Alzheimer's disease
Gene expression
RNA sequencing
Amyloid
APP23 mouse model
Inflammation

ABSTRACT

Aging is the key risk factor for Alzheimer's disease (AD). In addition, the amyloid-beta (Aβ) peptide is considered a critical neurotoxic agent in AD pathology. However, the connection between these factors is unclear. We aimed to provide an extensive characterization of the gene expression profiles of the amyloidosis APP23 model for AD and control mice and to evaluate the effect of aging on these profiles. We also correlated our findings to changes in soluble Aβ-levels and other pathological and symptomatic features of the model. We observed a clear biphasic expression profile. The first phase displayed a maturation profile, which resembled features found in young carriers of familial AD mutations. The second phase reflected aging processes and showed similarities to the progression of human AD pathology. During this phase, the model displayed a clear upregulation of microglial activation and lysosomal pathways and downregulation of neuron differentiation and axon guidance pathways. Interestingly, the changes in expression were all correlated to aging in general, but appeared more extensive/accelerated in APP23 mice.

1. Introduction

Dementia is considered to be one of the most burdensome disorders of later life. Aging is believed to be the main risk factor for dementia. No other disorders display higher age dependence than dementia [1]. Alzheimer's disease (AD) is believed to be the main cause of dementia. However, the proportion of cases caused by AD varies based on gender, age and whether mixed types of dementia are considered a separate subtype. Specifically, AD accounts for about 70% of all dementia at later age in women. In men, AD causes about 38% of all dementia between 65 and 69, but this percentage climbs progressively to 80% at 90 years and older [2]. AD is a neurodegenerative disorder causing progressive cognitive impairment and behavioural disturbances. The brain of AD patients is neuropathologically characterized by neuronal loss, gliosis, dystrophic neurites, amyloid plaques and neurofibrillary tangles of hyperphosphorylated tau [3]. Genetically, AD can be categorized into two distinct types: sporadic AD (SAD) and familial AD (FAD). SAD is considered to be a polygenic/multifactorial disorder and accounts for over 99% of all AD. While no clear genetic cause has been found for SAD, multiple genetic risk factors have been identified [4]. FAD, on the other hand, is caused by mutations inherited in an autosomal dominant fashion and accounts for <1% of all AD. FAD patients tend to display a relatively earlier age of onset, between 35 and 65 years of age, when compared to SAD. As a result, FAD is also often termed early-onset AD [5]. However, the majority of early-onset cases (i.e. onset before the age of 65) do not carry an FAD mutation and are, in fact, SAD cases. All known FAD mutations are located in one of three genes: the presenilin 1 (PSEN1), presenilin 2 (PSEN2) or the amyloid precursor protein (APP) gene [6–11]. Interestingly, all these genes play a crucial role in the production of the amyloid-beta (Aβ) peptide, the main component of the aforementioned amyloid plaques typically found in the brains of AD patients. The Aβ peptide has been found to vary in length between 37 and 43 amino acids. The most commonly produced variant is 40 amino acids in length ($A\beta_{1-40}$), but the Aβ variant with 42 amino acids ($A\beta_{1-42}$) is believed to be more prone to aggregation and, therefore, more neurotoxic [12–15]. FAD mutations have been shown to result in either an overall increase in Aβ production or a proportional shift towards the production of $A\beta_{1-42}$ [16–22]. Based on the genetic evidence, the neuropathological lesions and biochemical research confirming the

* Corresponding author at: Laboratory of Neurochemistry and Behavior, Institute Born-Bunge, University of Antwerp, Campus Drie Eiken, Universiteitsplein 1, 2610, Wilrijk, Antwerp, Belgium.
E-mail address: debby.vandam@uantwerpen.be (D. Van Dam).

http://dx.doi.org/10.1016/j.bbadis.2016.11.014
0925-4439/

neurotoxic properties of Aβ, the amyloid cascade hypothesis was formulated, which states that the Aβ peptide is a key factor in AD pathology [23,24]. Given this potentially central role of Aβ and the strong correlation between AD and aging, we decided to investigate the interaction between soluble Aβ levels and age in a transgenic mouse AD model [25]. Due to the inherent difficulties in studying brain disorders and the prolonged time course of AD pathology in humans, transgenic mouse models have proven an invaluable tool in AD research. The APP23 mouse model carries a construct containing the human APP_{751} gene with the Swedish double mutation (K670N/M671L) [26]. This is a known FAD mutation and results in an overall increase of Aβ production [22]. The model presents with neuropathological lesions, cognitive deficits and behavioural alterations in an age-dependent fashion, similar to human AD pathology [27,28]. Recently, we uncovered that the soluble Aβ levels in APP23 mice follow a distinct pattern over the course of their life. After an initial increase in the soluble overall Aβ and $Aβ_{1–40}$ levels at 1.5 months, the soluble Aβ levels remained stable until past 12 months of age. Only at the late ages of 18 and 24 months, could an additional, gradual increase in Aβ levels be detected. We also demonstrated that rises in overall Aβ and $Aβ_{1–40}$ levels are usually preceded by a rise in $Aβ_{1–42}$ levels. As the rise in Aβ levels at young age coincided with an increase in APP levels, this rise might simply reflect an evolution in Aβ production associated with brain maturation. However, we were unable to link the Aβ alterations at older ages to changes in the levels of proteins involved in the production of Aβ [25]. Of course, the activity of Aβ producing proteins may be altered by the aging process. Another explanation might be that the rise in Aβ levels at old age is the result of a reduction in Aβ clearance [29–35]. We, therefore, decided to use RNA sequencing to map other age-related changes in the expression profile of our mouse model. In our current study, we used differential expression analysis and weighted gene co-expression network analysis (WGCNA) to explore age-related and genotype-related changes in the APP23 mice. We also examined how these changes correlate to soluble Aβ levels. Finally, we also discuss how these findings relate to the pathological changes and AD-like symptoms observed at various ages in the APP23 model.

2. Materials and methods

2.1. Animals

Three male heterozygous (HET) APP23 mice were included in all age groups for the RNA sequencing analysis. An equal number of male wild-type (WT) littermates were included as a control group. Genotypes were determined through PCR. All mice were bred within our facilities on a C57Bl/6J background and group-housed in standard mouse cages under conventional laboratory conditions with a 12:12 h light–dark cycle (light on at 8:00 AM, light off at 8:00 PM), constant room temperature (22 ± 2 °C), humidity level (55 ± 5%), and food and water available ad libitum. Based on the timing of the previously observed changes in the soluble Aβ levels [25], four age groups were selected: 1.5, 6, 18 and 24 months. Experiments were conducted in accordance with the European Directive (2010/63/EU) on the protection of animals used for experimental and other scientific purposes, and the Animal Ethics Committee of the University of Antwerp approved all procedures.

2.2. Brain tissue collection

Animals were euthanized at the desired age through cervical dislocation. The brain was harvested and dissected on ice into three parts: two hemi-forebrains and the cerebellum (the olfactory bulbs were discarded). After dissection the brains were immediately stored at −80 °C until use. One hemi-forebrain was used for protein extraction and subsequent biochemical analysis. The other hemi-forebrain was used for RNA isolation and sequencing.

2.3. Protein extraction and ELISA

Proteins were extracted from the brain tissue and the Aβ levels ($Aβ_{1–x}$, $Aβ_{1–40}$ and $Aβ_{1–x}$) were determined through ELISA analysis according to the protocols previously described [25].

2.4. RNA isolation and sequencing

The frozen hemi-forebrains were lysed in QIAzol (Qiagen), followed by total RNA isolation using the RNeasy Lipid Tissue Mini Kit (Qiagen, 74804). The quality and concentration of the RNA was determined using the 2100 Bioanalyzer (Agilent, Amstelveen, The Netherlands) with the Agilent RNA 6000 Nano Kit and 3 high quality samples (RIN > 7.5) per condition were included for sequencing.

Sequence libraries were generated with the TruSeq RNA sample prep kit V2 (Illumina) using the Sciclone NGS liquid handler (Perkin Elmer). To multiplex the samples in two pools, 24 unique barcoded adapters (Illumina) were applied. The generated cDNA libraries were sequenced on an Illumina HiSeq2500 using default parameters (single read 50 base pairs in High Output modus).

2.5. Bioinformatic data preprocessing

The data was inspected with FASTQC (v0.10.1) [Babraham institute, available online at: http://www.bioinformatics.babraham.ac.uk/projects/fastqc/] and trimmed when necessary with FASTX trimmer [Hannon Lab, available online at: http://hannonlab.cshl.edu/fastx_toolkit/]. Alignment was performed with STAR (2.3.1 l) [36] with 2 mismatches allowed to the ensemble reference genome version 37 of the 1000Genome project. Between 10 and 16 million high-quality uniquely aligned reads were obtained per sample. Data was quantified with HT-Seq count (0.5.4) [37]. The complete dataset was uploaded to the GEO repository of the National Center for Biotechnology Information (NCBI) and are accessible through GEO Series accession number: GSE80465.

2.6. Differential genes expression analysis

The raw count data were preprocessed with the use of the programming language R (3.2.2) [R Core Team, 2015, available online at: www.r-project.org], the program RStudio (0.99.484) [RStudio Team, 2015, available online at: http://www.rstudio.com/] and the EdgeR package (3.12) [38]. Genes that contained a count per million (CPM) value >1 in at least two samples were kept resulting in 15,728 genes that were used in the differential analysis. Differential expression of the data was performed by pairwise comparisons, as well as a generalized linear model with genotype and age as main variables and a genotype * age interaction variable. The generalized linear model (GLM) approach was applied to both genotypes of the 1.5 and 6 month old animals (maturation design) and to both genotypes of the 6, 18 and 24 month old animals (aging design). In the aging design, age was used as a quantitative variable. The "false discovery rate" (FDR) method was used to statistically correct for multiple comparisons.

2.7. Weighted gene co-expression network analysis (WGCNA)

WGCNA (1.48) [39,40] was applied to identify modules of highly co-expressed genes. Genes of which the mean CPM expression values were below the 25% quartile where removed, resulting in a co-expression matrix of 11,796 genes. A signed network was generated with a beta value of 10, and after clustering of the genes in modules only modules of 100 genes or more were used for downstream analysis. Highly correlating modules were merged with the WGCNA MergeCloseModules function with a cutoff of 0.25. ModuleTrait correlations were calculated between the modules and 5 predictive variables: Genotype, Age,

Maturation, APP23-Aging and WT-Aging. The APP-Aging and WT-Aging variables contained the various ages of the animals for that particular genotype, while the other genotype was maintained at 1.5 months, in order to identify genotype-specific age-related modules. In addition, the ModuleTrait relationships between the modules and the observed, soluble Aβ levels was also determined.

To functionally annotate the modules and the differentially expressed gene lists DAVID was used [41,42]. In addition, the WGCNA userlistEnrichment function was applied to functionally annotate the modules [43]. This function contains an extensive CNS cell type-specific gene expression profiles.

3. Results

3.1. The APP23 transcriptome profile

To determine the effect of age and mutated APP overexpression on gene expression levels in the central nervous system, Illumina RNA-sequencing was applied to one hemi-forebrain of APP23 and WT animals aged 1.5, 6, 18 and 24 months. The relationships between the samples and conditions were visualized in a multi-dimensional scaling (MDS) plot (Fig. 1A). The MDS plot confirmed that the different biological triplicates cluster closely together.

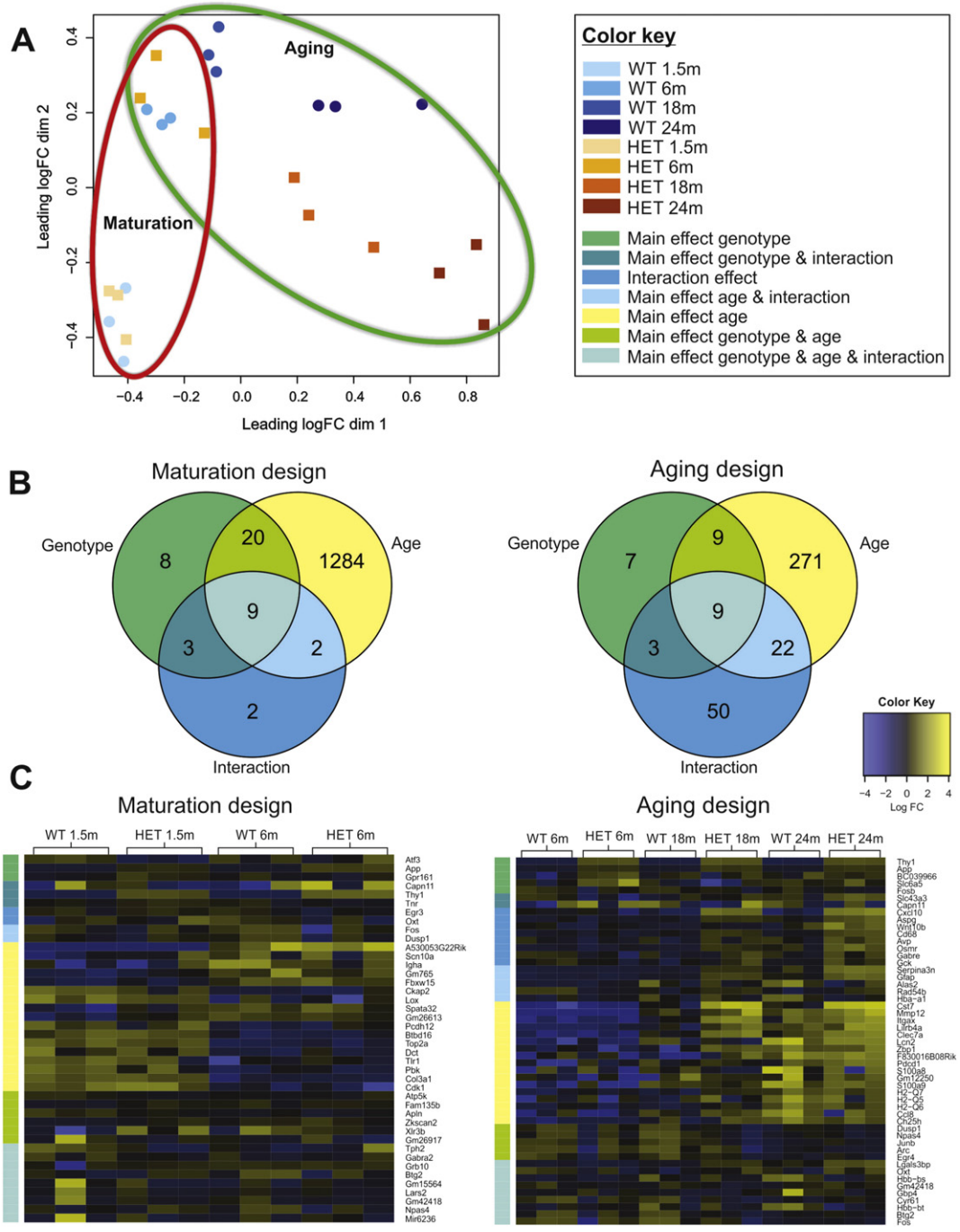

Fig. 1. Results of differential gene expression analysis. A) Multi-dimensional scaling plot displaying the results for the various age and genotype groups. The two main trends, maturation and aging, are indicated by a red and green circle, respectively. B) Venn diagrams displaying the numbers of differentially expressed genes grouped according to their association with the variables in the two generalized linear model designs. C) Heatmaps depicting the top differentially-expressed genes for the main effects of aging, genotype, and the age-genotype interaction effect for the maturation and aging designs. These top genes are categorized according to unique and significant associations with main variables. Abbreviations: HET, heterozygote; WT, wild-type; m, months.

In addition, two global trends could be observed, as indicated by the two circles on the plot. The youngest WT and HET groups cluster together at the lower left corner, whereas the 6-month-old WT and HET groups are clustered in the top left-hand corner. This initial upward trend appears to occur specifically between the two youngest age groups and was categorized as the maturation profile (the red circle). The oldest age groups, on the other hand, display a shift downward and to the right. This trend, involving the 6-, 18- and 24-month age groups, was classified as the aging profile (the green circle). This aging effect is most pronounced in the APP23 group, resulting in an increasing divergence between the HET and WT animals.

The differential expression of genes was initially assessed by a simple pairwise comparison between the various experimental groups. The number of genes that significantly differ in expression between two particular experimental groups (FDR < 0.05) are reported in Tables 1 and 2. Interestingly, these comparisons showed that at 6 months of age the only two differentially expressed genes are *APP* and *Thy1*, both of which are components of the construct introduced in the APP23 model. The expression level of both genes appears to increase in HET animals at the earliest ages, before levelling out at a later age. In accordance with what we observed in the MDS-plot, the number of genes differentially expressed between WT and HET rises with increasing age. Within a given genotype group most of the expression changes appear to occur early or late in life.

3.2. The generalized linear model analysis

The GLM designs were used for further analysis of the differential expression. Based on the previously observed profiles, two GLM designs were developed: a maturation design containing APP23 and WT mice of 1.5 (juvenile) and 6 months (adult) of age and an aging design that contained APP23 and WT mice of 6, 18 and 24 months. The 6-month-old group is considered a turning point and was included in both designs as a reference group (when the differences in expression between APP23 and WT mice are minimal and restricted to the introduced construct). The designs examine which gene expression changes are due to the effect of aging, the effect of genotype or an interaction between the two.

For the maturation design, 40 genes were differentially expressed between genotypes, 1315 genes differed between 1.5 and 6 month old mice, and 16 genes were significantly associated with the interaction effect (FDR < 0.05) (Suppl. Tables 1–3). Several genes were also overlapping between these effects (Fig. 1B); for example, 9 genes were significantly associated with age, genotype and the interaction effect. Together, these results indicate that changes in gene expression levels were most strongly affected by maturation, and that the difference between genotypes, and the difference in the maturation profile between both genotypes, were relatively minor.

Similarly, a GLM approach was applied to the aging design containing the samples from the 6-, 18- and 24-month-old mice. The expression of 28 genes was affected by genotype, 311 genes were affected by age, and 84 genes associated with the interaction effect (Suppl. Tables 4–6). These findings indicate that the effect of age in the aging design is much less pronounced than in the maturation design (311 versus 1315 affected genes). Interestingly, the interaction between age and genotype effect is more pronounced for the aging design (84 versus 16 genes). This again suggests that in APP23 samples, gene expression levels become increasingly different from control littermates with progressive age.

Table 1
Differentially expressed genes in HET animals compared to WT animals.

Age	#Total	#Upregulated	#Downregulated
2 M	8	6	2
6 M	2	2	–
18 M	189	166	23
24 M	422	215	207

Abbreviations: HET, heterozygous; WT, wild-type; M, months.

Table 2
Differentially expressed genes between 2 age groups of the same genotype.

Ages	WT			HET		
	#Total	#Up	#Down	#Total	#Up	#Down
2 M compared to 6 M	1277	708	569	731	469	262
6 M compared to 18 M	50	19	31	280	42	238
18 M compared to 24 M	398	168	230	858	439	419

Abbreviations: HET, heterozygous; WT, wild-type; M, months.

Heatmaps were generated that depict the principal differentially-expressed genes for the main effects of aging, genotype, and the age-genotype interaction effect for the maturation and aging designs (Fig. 1C). These top genes were subsequently categorized according to unique and significant associations with main variable of age (yellow), genotype (green) or interaction effect (blue) or to a combination of these; age and genotype (light green), age and interaction (light blue); genotype and interaction (dark green), or all three effects (light bluegreen), in analogy to the categories visualized in the Venn diagrams in Fig. 1B.

As expected, the category genotype-unique for both the maturation and aging designs contained the *APP* gene, the gene responsible for inducing the pathology in APP23 mice. Interestingly, the *Thy1* gene, which drives the expression of the *APP* gene in the construct, was also found in the genotype-unique category of the aging design. In the maturation design, however, an interaction effect could be observed in addition to the genotype effect, indicating that the *Thy1* expression changes with age during the maturation stage. For the aging design, *Cd68* was present in the interaction-unique category. *Cd68*, a marker for activated microglia, was increased in expression in aged APP23 mice specifically. Similarly, *Gfap*, a marker of activated astrocytes, was present in the combined interaction and age effects, suggesting age-related astrocytosis which was more pronounced in APP23 mice. In addition, several microglia genes were detected in the main effect of the age-unique category, such as *Cd11c*, *Mmp12*, *Clec7a*, *H2-Q5*, *H2-Q6* and *H2-Q7*. Moreover, *Lgals3bp* was observed in the combined main effects and interaction effect category.

Given this study's focus on aging effects, functional enrichment analysis was performed on the aging design for genes significantly associated with the main effect of age and the age-genotype interaction effect (Table 3). The top GO term that was enriched for the age effect was 'Immune Response' (Benjamini $p = 4.3E^{-19}$), and the top GO term for the interaction effect was 'Acute inflammatory response' (Benjamini $p = 2.4E^{-03}$). These observations are in line with the heatmap, suggesting that there is an age-related increase in inflammatory genes, which was more pronounced in APP23 mice. KEGG pathway analysis revealed the complement and coagulation pathway (Benjamini $p = 5.5E^{-03}$) and the lysosome pathway (Benjamini $p = 4.5E^{-05}$) as top results for the main effect of age and the age-genotype interaction effect, respectively.

3.3. Weighted gene co-expression network analysis (WGCNA)

In addition to a differential expression analysis, a WGCNA-based clustering analysis was performed to detect groups of co-expressed genes that differed between conditions. A dendrogram was generated with branches of highly correlating genes that were identified as modules (Fig. 2A). The Module Eigengene (ME), the first principal component of the eight identified modules, was subsequently correlated to predictive variables to determine the expression of the modules (Fig. 2B). Five predictive variables were included in this analysis: genotype, age, maturation, and two interaction variables APP23-Aging and

Table 3
Results of the functional annotation of differentially expressed genes using DAVID.

	GO	Benjamini	KEGG	Benjamini
Main effect age (*aging design*)	Immune response	4.3E − 19	Complement and coagulation cascades	5.5E − 03
	Immune effector process	1.6E − 10	Antigen processing and presentation	7.3E − 03
	Leukocyte-mediated immunity	9.5E − 08	Systemic lupus erythematosus	2.5E − 02
Interaction effect (*aging design*)	Acute inflammatory response	2.4E − 03	Lysosome	4.5E − 05
	B-cell mediated immunity	3.4E − 03	Complement and coagulation cascades	4.0E − 02
	Immunoglobulin-mediated immune response	3.9E − 03	Systemic lupus erythematosus	8.3E − 02

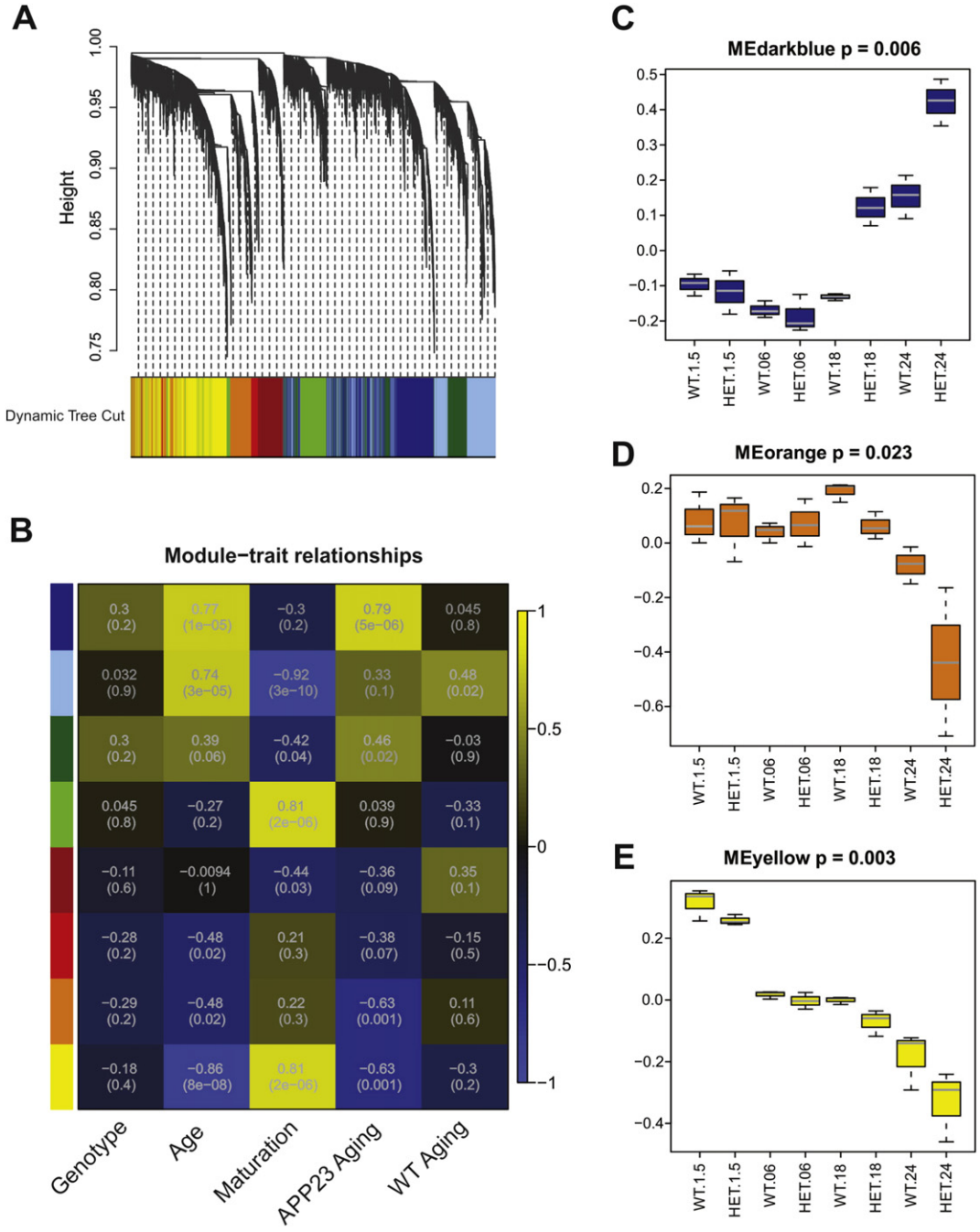

Fig. 2. Results of the weighted gene co-expression network analysis. A) Cluster dendrogram depicting the identified modules of highly correlating genes. B) Heatmap displaying the correlations (r- and *p*-values) between the gene modules and the five predictive variables. C) Boxplot depicting the Module Eigengene expression levels of the 'darkblue' module for the various experimental groups. D) Boxplot depicting the Module Eigengene expression levels of the orange module for the various experimental groups. E) Boxplot depicting the Module Eigengene expression levels of the 'yellow' module for the various experimental groups. Abbreviations: HET, heterozygote; WT, wild-type; ME, Module Eigengene.

WT-Aging. The five modules that significantly associated ($p < 0.005$) with one or more of these variables were: 'darkblue', 'lightgreen', 'lightblue', 'orange' and 'yellow'. No modules significantly associated with genotype or the interaction variable WT-Aging.

The 'lightgreen' module significantly and positively correlated with the 'maturation' variable ($R = 0.81$; $p = 2E^{-06}$) suggesting that this group of genes was highly expressed during maturation compared to adult mice (Fig. 2B). It is enriched for an 'astrocytes' gene set from [109] (Benjamini $p = 2.8E^{-18}$) and the 'Blood vessel development' GO category (Benjamini $p = 2.4E^{-08}$) (Suppl. Table 7). The 'lightblue' module negatively correlated with the 'maturation' variable ($R = -0.92$; $p = 3E^{-10}$) and positively with the 'age' variable ($R = 0.74$; $p = 3E^{-05}$), suggesting an age-related increase (Fig. 2B). It is enriched for the 'Calcium signalling' KEGG pathway (Benjamini $p = 2.1E^{-02}$) (Suppl. Table 7). Neither the 'lightgreen', nor the 'lightblue' module displayed any effects related to genotype.

The 'orange' module correlated negatively to the 'APP23-aging' interaction variable ($R = -0.63$; $p = 0.0001$) (Fig. 2B). The 'orange' ME only showed a profound down-regulation in 24-month-old APP23 mice (Fig. 2D). This module is enriched for a 'transcription' GO and a 'synaptic transcriptome' gene set from Cajigas and co-workers (Benjamini $p = 1.9E^{-07}$) (Table 4) [44], suggesting that synaptic composition is altered in APP23 mice aged 24 months. This is the only module that does not show an overall aging effect in addition to an interaction effect.

The 'darkblue' module correlated positively with the 'age' ($R = 0.77$; $p = 1E^{-05}$) and 'APP23-Aging' ($R = 0.79$; $p = 5E^{-06}$) variables, suggesting age-related alterations in gene expression, which are modified further in APP23 mice (Fig. 2B). The ME of the 'darkblue' module was depicted as a boxplot (Fig. 2C), and showed an age-related increase, which was more pronounced or potentially expedited in the APP23 mice. This module was enriched for 'immune response' GO-term (Benjamini $p = 9.5E^{-28}$), 'Lysosome' KEGG pathway (Benjamini $p = 6.1E^{-04}$), and 'microglia' gene set of userlistEnrichment (UE) (Benjamini $p = 1.2E^{-24}$) (Table 4). These observations are in line with the results from the GLM analysis. A variety of cathepsins, which are involved in lysosomal protein degradation, are prominently represented in the module. Interestingly, this module also contains most of the SAD genetic risk factors that have been linked to microglial activation, like Triggering Receptor Expressed on Myeloid cells2 (*Trem2*) and its co-receptor TYRO Protein Tyrosine Kinase Binding Protein (*Tyrobp*), *Cd33*, ATP-binding cassette transporter A 7 (*Abca7*), Inositol Polyphosphate-5-Phosphatase (*Inpp5d*) and apolipoprotein E (*Apoe*).

Table 4
Results of functional annotation and userlistEnrichment of WGCNA modules.

Module	Gene number	Dataset	Description	Benjamini
Darkblue	2375	GO	Immune response	9.5E−28
			Innate immune response	5.7E−13
		KEGG	Ribosome	4.3E−05
			Lysosome	6.1E−04
		UE	Microglia	1.2E−24
			Immune system reactome	4.3E−12
Orange	982	GO	Transcription	1.5E−02
			Protein amino acid dephosphorylation	6.7E−02
		UE	Synaptic transcriptome [44]	1.9E−07
Yellow	2167	GO	Neuron differentiation	6.0E−03
			Transmission of nerve impulse	2.9E−02
		KEGG	Pathways in cancer	7.7E−05
			Axon guidance	4.1E−03

Abbreviation: WGCNA, weighted gene co-expression network analysis; UE, userlistEnrichment.

Complement receptor 1 (*Cr1*), another risk factor that has also been linked to the immune system, was not found in this module, but several other subcomponents of the first component of the complement system were (i.e. *C1qa*, *C1qb*, *C1qc* and *C1ra*).

The 'yellow' module positively correlated to 'maturation' ($R = 0.81$; $p = 2E^{-06}$), and negatively to 'age' ($R = -0.86$; $p = 8E^{-08}$), and 'APP23-aging' ($R = -0.63$; $p = 0.001$) variables (Fig. 2B). The ME of the 'yellow' module was highest in immature animals with age-related decrease, which was most prominent in the APP23 mice (Fig. 2E). This module is, among others, enriched for 'neuron differentiation' − GO (Benjamini $p = 6.0E^{-03}$) and 'axon guidance' − KEGG (Benjamini $p = 4.1E^{-03}$) gene sets (Table 4). This suggested an age-related decrease in axonal guidance and neuronal differentiation signalling genes, which was most pronounced in APP23 mice. Fermitin Family Member 2 (*Fermt2*), a SAD risk gene linked to cytoskeletal function and axonal transport, was also found in this module.

Finally, we explored the relationship between the ME of these modules and the brain Aβ levels that were measured in these animals. Interestingly, the strongest significant correlations were observed with the overall $A\beta_{1-x}$ levels (Suppl. Fig. 1). The 'darkblue' and 'orange' module, respectively, displayed the highest positive ($R = 0.69$; $p = 2E^{-04}$) and negative correlation ($R = -0.66$; $p = 4E^{-04}$) to the $A\beta_{1-x}$ levels. In addition, these modules also displayed a similar, but weaker correlation to the $A\beta_{1-40}$ levels ('darkblue': $R = 0.6$; $p = 0.002$, 'orange': $R = -0.58$; $p = 0.003$). Surprisingly, a positive correlation was also found between the $A\beta_{1-x}$ levels and the 'darkgreen' module ($R = 0.60$; $p = 0.002$). This module did not relate to our other variables and appears to be enriched for 'DNA metabolic processes' and 'DNA repair' GO gene sets (Suppl. Table 7). Finally, the 'yellow' module also showed a negative correlation with the $A\beta_{1-x}$ levels ($R = -0.59$; $p = 0.002$). The correlations between the modules and the $A\beta_{1-42}$ levels failed to reach the significance level ($p < 0.005$).

4. Discussion

The goal of this study was to examine the role of aging and age-related changes in gene expression in the APP23 mouse model for AD. Overall, our study revealed a very distinct pattern in the gene expression profile. We observed an initial, maturation stage at the youngest ages with a large amount of changes in gene expression. Notably, our GLM analysis showed that the vast majority of these changes are age-related and only ~3% of the changes are linked to the genotype. Moreover, the WGCNA analysis also revealed three modules that correlated with maturation, but none of these modules appeared to be affected by the genotype variable. In fact, given that these modules have functional annotations like 'neuron differentiation', 'axon guidance' and 'blood vessel development', their involvement in this maturation phase is quite logical. Actually, during the maturation stage, the differences between WT and HET appear to diminish until at 6 months the only significantly differentially expressed genes between both groups are the *APP* and *Thy1*-gene of the transgenic construct. Our analyses show that the expression level of both these genes increases during the initial maturation stage and reaches an elevated, steady state at later ages. In a previous study, we also observed an increase in the protein levels of APP between the age of 1.5 and 6 months after which they levelled out [25]. These findings seem to confirm our previous hypothesis that a further maturation of the brain takes place in juvenile APP23 mice which may be the cause of the initial rise in soluble Aβ levels observed in the model.

The existence of this maturation stage does, however, raise some interesting issues about the interpretation of findings at these young ages. For instance, young APP23 animals up to the age of 8 months have been shown to have 10–15% more neurons compared to controls and older APP23 animals [45,46]. This augmented volume of specific brain regions has also been observed in young human FAD carriers and has been linked to differences in functional connectivity [47,48]. It is unclear,

Table 5
Differences observed in heterozygous APP23 mice compared to wild-type control animals.

Observation	Age(s) tested	First detected	Evolution	Reference(s)
Pathological hallmarks:				
Dense core plaques	3 m, 6 m, 8 m, 12 m, 19 m, 24 m, 25 m	6 m	Progressive; plaques increase and spread	26, 27, 64
Diffuse plaques	14–18 m	14 m	Limited, specific brain regions, most common with high plaque burden, <10% of plaque total	46
Cerebral amyloid angiopathy	8 m, 14–21 m, 19 m, 27 m	14 m	Progressive; Starts in leptomeningeal vessels	69, 70
Hyperphosphorylated tau	6 m,9 m,12 m,15 m,18 m, 24 m	6 m	Progressive; occurs parallel with plaque deposition	26, 27
Dystrophic neurites & axonal sprouting	6 m,9 m,12 m,15 m,18 m, 24 m	6 m	Progressive; occurs around dense core plaques	26, 27
Inflammatory response	4–9 m, 6 m, 9 m, 12 m, 14–18 m, 15 m, 15–20 m, 16 m,18 m, 20 m 24 m	6 m	Progressive; occurs around dense core plaques	26, 27, 61, 63, 75
Higher number of neocortical neurons	2 m, 8 m, 14–18 m, 27 m	2 m	Difference disappears with age. No difference past 14–18 m. Correlates with plaque load.	45, 46
Neuronal loss in CA1	14–18 m	14 m	Increases; correlates with plaque load	46
Disrupted synaptic function (CA1)	3 m, 6 m, 9 m, 12 m, 18 m, 24 m	12 m	Largest at 18 m; no detectable difference at 24 m	71
Altered neurotransmitter levels	7–8 m	7–8 m	Differences in cholinergic, noradrenergic, serotonergic systems + glycine and inhibitory amino acid levels	67
Deterioration of the cholinergic system	6 m, 15 m, 24 m	15 m	Decrease in cholinergic enzyme activity and fiber length	68
Cognitive deficits:				
Reduced MWM performance	6–8w, 3 m, 6 m, 16 m, 18 m, 24 m, 25 m	3 m	No change observed beyond 3 m until 25 m	53, 56, 57, 59
Passive avoidance learning diminished	6–8w, 3 m, 6 m, 18 m 25 m	25 m	NA	53, 57
Slower learning in plus shaped water maze	6 m	6 m	NA	54
Impeded complex maze performance	10 m	10 m	NA	58
Impaired Barnes maze learning	12 m	12 m	NA	55
Behavioural changes:				
Altered cage activity profile	3 m, 6 m, 12 m	6 m	Changes more pronounced at 12 m	72
Hyperactivity	6–8w, 3 m, 6 m	6–8w	No evolution observed	53
Increased aggression	6 m, 12 m	6 m	No evolution observed	73

Abbreviation: m, months; MWM, Morris water maze; NA, not available; w, weeks.

however, to what extent these changes should be considered a developmental difference or a part of AD pathology. Both APP and presenilins have been shown to play a part in neuronal development under normal physiological circumstances and mutations in these genes may affect their ability to optimally perform their normal function [49–52]. This may, however, be unrelated to other pathological effects, like Aβ toxicity for example. The first cognitive deficits in APP23 mice have been observed at the age of three months [53] (Table 5). In the light of these discoveries, we have to ask ourselves if this diminished performance in the Morris water maze is an early, pathological deterioration of higher order brain function, comparable to the mild deficits observed in the earliest disease stages, or is it in fact the result of a deviation in brain development. The age at which cognitive deficits are first detected in the APP23 model has proven to be highly dependent upon the experimental set-up used in the testing. In general, however, complex cognitive tasks do seem to be impaired earlier than simpler memory tasks, similar to the progression of cognitive decline in human AD patients [53–59]. In the end, the APP23 model does appear to mimic the progressive cognitive deterioration of the human condition, but the earliest observed cognitive deficits may not necessarily reflect the first observable cognitive deficits in humans and should, therefore, be interpreted with caution. While these changes in young APP23 mice seem to correlate well with the situation in young human FAD patients, they may relate poorly to SAD and could seriously impact the potential extrapolation of research results.

Nevertheless, in addition to the maturation phase of the gene expression profile, we also observed an aging phase. Starting at 6 months of age with minimal gene expression differences between WT and HET animals, we determined an ever increasing number of alterations in gene expression and an increasing divergence between both genotypes with increasing age. At 6 months of age, the first sporadic, compact plaques can be observed in the APP23 model. These plaques are accompanied by local changes, like activated microglia, hypertrophic astrocytes, axonal sprouting and dystrophic neurites [26,27,60–64] (Table 5). In human pathology these first alterations are believed to occur during the preclinical stage, before the onset of symptoms [65]. The average age of onset for carriers of an APP mutation in humans is just under 50 years of age [5]. In C57BL/6J mice the equivalent age for this human age is estimated at ~14 months. The human age equivalent for mice aged 6 months is believed to be 30 years [66]. Based on the human equivalent ages, the 6-month-old mice would indeed be expected to correspond with humans in the presymptomatic stage. Unlike humans in this presymptomatic stage, cognitive deficits have been observed in APP23 mice at 6 months [53,57]. However, to date there is no other experimental evidence to support that this cognitive deficit has progressed beyond the deficit that was detected at 3 months during the previously discussed maturation stage. In fact, the only additional worsening of cognitive symptoms in APP23 mice has been observed at the late age of 25 months in a small Morris water maze and the passive avoidance test [57] (Table 5). Similarly, deviations in the neurotransmitter systems were found in APP23 mice at the age of 6 months compared to WT littermates [67]. However, these alterations were again not shown to progressively worsen over time. One study did note a progressive deterioration of the cholinergic system, but these changes were reported after 6 months. They reported minor changes at 15 months that became more extensive at 24 months [68] (Table 5). Other pathological features, like hippocampal neuronal loss and vascular amyloid deposition, have also been reported at 14 months and were shown to exacerbate at later ages [45,46,69,70] (Table 5). Basic synaptic function is reportedly mildly altered at 12 months of age and more extensively modified at 18 months in the APP23 model [71]. At 6 months of age, the spontaneous home cage locomotor activity profile of APP23 mice was found to display minor differences compared to the profile of wild-type controls, and these differences became more pronounced at 12 months [72]. Other behavioural disturbances in activity and aggression have also been reported, even before age 6 months, but no progression of these symptoms has been documented [53,73] (Table 5). Taken together, these findings appear to confirm the progression of AD-like pathology during the aging stage in the APP23 model. The timing of the pathological features during this stage also seems to match the timing of the pathology in human FAD patients.

Our WGCNA analysis revealed three modules that display clear changes in gene expression during the aging stage: the 'darkblue',

'yellow' and 'orange' modules. Interestingly, none of these modules displays gene expression changes that are solely due to genotype effects. All of the observed variations in gene expression do correlate to aging. In fact, the 'darkblue' and 'yellow' modules both exhibit an aging effect independent of genotype, indicating that these modules are also altered with aging in WT animals. However, the alterations of these modules in APP23 mice appear to precede or exceed the changes in the WT animals. At 18 months, the expression levels of the 'darkblue' and 'yellow' modules differ significantly in APP23 compared to age matched controls and younger APP23 mice. These changes become even more prominent at 24 months. At this age, modifications in these modules can also be observed in WT animals. The changes in expression in the APP23 mice appear to follow the same temporal pattern as the one previously observed for the soluble $A\beta_{1-42}$ levels [25]. These similarities are, however, not reflected in our correlation analysis of the soluble Aβ levels and the ME of these modules. Our correlation analysis seems to pick up the more prominent alterations at 24 months, but may lack sufficient power to detect the more modest effects at 18 months. Overall, the aging stage of the APP23 model is characterized by accelerated age-related alterations in gene expression and these accelerated changes appear associated with the rising levels of soluble Aβ and the appearance of AD-like brain pathology.

The functional annotations of the three modified modules could, therefore, provide valuable insights into the molecular processes involved in the observed pathological changes. The 'darkblue' module displays a clear association with immunological processes and enrichment for the microglia gene set. This upregulation of immune-related genes was also found in the GLM analysis and contain genes that previously have been linked by our group to microglia priming [74]. Recently, our group also microscopically confirmed the presence of primed microglia in the vicinity of plaques at 16 months of age in the APP23 model. At 24 months, priming could also be observed in non-plaque regions and WT animals as well [75]. These results are in line with our current observations and with other studies reporting immune system activation in the brains of both human AD patients and mouse models [76–81]. Similar to our findings in old WT animals, aging in humans has also been associated with immune system dysregulation (immunosenescence) and chronic low-grade inflammation (inflammaging) [82–84]. Activated microglia are involved in phagocytic clearance of pathogens and debris and are responsible for the subsequent lysosomal degradation [74,80]. Our 'darkblue' module was also significantly enriched for the 'lysosomal' KEGG pathway and the SAD risk genes it contained have also been linked to phagocytosis (as reviewed in [85]). Despite the apparent increase in microglial activation, several studies have shown that these microglia may be functionally impaired, displaying decreased mobility and phagocytic capacity [86–90]. Phagocytosis and lysosomal degradation by proteases like cathepsins may play a role in Aβ clearance and changes in these systems could therefore contribute to the observed accumulation of soluble Aβ [91–94]. At the moment, it is still unclear to what extent the microglial activation occurs as compensatory immune response to the increasing amyloid load or as a normal part of the aging process which might contribute to the AD pathology.

The 'yellow' module of our WGCNA analysis is functionally annotated for 'neuron differentiation' and the 'axon guidance' pathway. This generally down-regulated module contains the genes of axonal guidance cues like netrins, ephrins, slits, semaphorins and their receptors, as well as the genes of their downstream proteins Ras, Pak and Rock. Together, these elements of the 'axon guidance' pathway are responsible for the regulation of the actin cytoskeleton. This regulatory mechanism plays a crucial role in the morphogenesis of dendritic spines and regulation of synaptic plasticity [95–97]. Moreover, Aβ and sAPPα have been shown to interact with ephrin and semaphorin receptors, respectively [98–101]. Aβ oligomers have also been shown to lead to aberrant Pak activation and downstream modification of the actin cytoskeleton and dendritic spines [102,103]. These modifications in the regulation of the actin cytoskeleton have been found both in AD mouse models and human AD brain [104–107]. Impairments in the axon guidance pathway could explain the changes in basic synaptic function and may lead to the deterioration of cognition in the APP23 model at old age. Interestingly, actin cytoskeleton regulation also plays a crucial role in phagocytosis (as reviewed in [108]) and could provide a link between the changes observed in neurons and microglia.

Finally, we also observed changes in the 'orange' module, which was annotated for the 'synaptic transcriptome' and transcription. Unlike the 'yellow' and 'darkblue' module, this module did not display an overall aging effect. Based on the timing of the observed changes, it would appear that these changes in transcription at the synaptic level are a consequence of earlier pathological effects. In this study, we performed a global screening in the entire hemi-forebrain in accordance with our previous experiments in APP23 mice [25]. Future research, could provide additional information about more modest changes, which might have been masked or diluted with this approach, by performing region- or cell type-specific analyses.

5. Conclusion

In conclusion, our study has shown a clear biphasic evolution in gene expression changes in the APP23 model over time. While the initial, maturation phase shares certain similarities with young FAD carriers, it may not be representative for the pathological AD processes that occur at later age in FAD and SAD patients. The second phase, however, mimics several prominent features of the progressive AD pathology, both in FAD and SAD. Our results show that aging is the crucial factor during the second phase. The gene expression modules displaying the most prominent alterations in APP23 mice, are also affected in WT animals, but the age-related changes appear accelerated/exacerbated in APP23 mice. These findings should be taken into account during the selection of age groups for future research. The APP23 model does appear to be a valid model to further investigate the relationship between aging and AD pathology. Microglial function and, perhaps more importantly, cytoskeletal regulation pathways would appear to be the most interesting targets for these future investigations.

Transparency document

The Transparency document associated with this article can be found, in online version.

Acknowledgements

This work was supported by the Research Foundation-Flanders (FWO), "Stichting voor Alzheimer Onderzoek" (SAO), (S#15002) — "Foundation pour la Recherche sur la Maladie d'Alzheimer" (FRMA), Interuniversity Poles of Attraction (IAP Network P7/16) of the Belgian Federal Science Policy Office, Methusalem excellence grant of the Flemish Government, agreement between Institute Born-Bunge and University of Antwerp, the Medical Research Foundation Antwerp, the Thomas Riellaerts research fund, and Neurosearch Antwerp.

Appendix A. Supplementary data

Supplementary data to this article can be found online at http://dx.doi.org/10.1016/j.bbadis.2016.11.014.

References

[1] M.J. Prince, F. Wu, Y.F. Guo, L.M.G. Robledo, M. O'Donnell, R. Sullivan, S. Yusuf, The burden of disease in older people and implications for health policy and practice, Lancet 385 (2015) 549–562.
[2] WHO, Dementia: A Public Health Priority, World Health Organization, Geneva, 2012.

[3] A. Serrano-Pozo, M.P. Frosch, E. Masliah, B.T. Hyman, Neuropathological alterations in Alzheimer disease, Cold Spring Harb. Perspect. Med. 1 (2011) a006189.
[4] E. Bagyinszky, Y.C. Youn, S.S. An, S. Kim, The genetics of Alzheimer's disease, Clin. Interv. Aging 9 (2014) 535–551.
[5] D.C. Ryman, N. Acosta-Baena, P.S. Aisen, T. Bird, A. Danek, N.C. Fox, A. Goate, P. Frommelt, B. Ghetti, J.B. Langbaum, F. Lopera, R. Martins, C.L. Masters, R.P. Mayeux, E. McDade, S. Moreno, E.M. Reiman, J.M. Ringman, S. Salloway, P.R. Schofield, R. Sperling, P.N. Tariot, C. Xiong, J.C. Morris, R.J. Bateman, N. Dominantly, Inherited Alzheimer, symptom onset in autosomal dominant Alzheimer disease: a systematic review and meta-analysis, Neurology 83 (2014) 253–260.
[6] E. Levy, M.D. Carman, I.J. Fernandez-Madrid, M.D. Power, I. Lieberburg, S.G. van Duinen, G.T. Bots, W. Luyendijk, B. Frangione, Mutation of the Alzheimer's disease amyloid gene in hereditary cerebral hemorrhage, Dutch type, Science 248 (1990) 1124–1126.
[7] E. Levy-Lahad, W. Wasco, P. Poorkaj, D.M. Romano, J. Oshima, W.H. Pettingell, C.E. Yu, P.D. Jondro, S.D. Schmidt, K. Wang, et al., Candidate gene for the chromosome 1 familial Alzheimer's disease locus, Science 269 (1995) 973–977.
[8] M.C. Chartier-Harlin, F. Crawford, H. Houlden, A. Warren, D. Hughes, L. Fidani, A. Goate, M. Rossor, P. Roques, J. Hardy, et al., Early-onset Alzheimer's disease caused by mutations at codon 717 of the beta-amyloid precursor protein gene, Nature 353 (1991) 844–846.
[9] A. Goate, M.C. Chartier-Harlin, M. Mullan, J. Brown, F. Crawford, L. Fidani, L. Giuffra, A. Haynes, N. Irving, L. James, et al., Segregation of a missense mutation in the amyloid precursor protein gene with familial Alzheimer's disease, Nature 349 (1991) 704–706.
[10] E.I. Rogaev, R. Sherrington, E.A. Rogaeva, G. Levesque, M. Ikeda, Y. Liang, H. Chi, C. Lin, K. Holman, T. Tsuda, et al., Familial Alzheimer's disease in kindreds with missense mutations in a gene on chromosome 1 related to the Alzheimer's disease type 3 gene, Nature 376 (1995) 775–778.
[11] R. Sherrington, E.I. Rogaev, Y. Liang, E.A. Rogaeva, G. Levesque, M. Ikeda, H. Chi, C. Lin, G. Li, K. Holman, T. Tsuda, L. Mar, J.F. Foncin, A.C. Bruni, M.P. Montesi, S. Sorbi, I. Rainero, L. Pinessi, L. Nee, I. Chumakov, D. Pollen, A. Brookes, P. Sanseau, R.J. Polinsky, W. Wasco, H.A. Da Silva, J.L. Haines, M.A. Perkicak-Vance, R.E. Tanzi, A.D. Roses, P.E. Fraser, J.M. Rommens, P.H.S. George-Hyslop, Cloning of a gene bearing missense mutations in early-onset familial Alzheimer's disease, Nature 375 (1995) 754–760.
[12] D. Burdick, B. Soreghan, M. Kwon, J. Kosmoski, M. Knauer, A. Henschen, J. Yates, C. Cotman, C. Glabe, Assembly and aggregation properties of synthetic Alzheimer's A4/beta amyloid peptide analogs, J. Biol. Chem. 267 (1992) 546–554.
[13] J.T. Jarrett, E.P. Berger, P.T. Lansbury Jr., The carboxy terminus of the beta amyloid protein is critical for the seeding of amyloid formation: implications for the pathogenesis of Alzheimer's disease, Biochemistry 32 (1993) 4693–4697.
[14] M. Bibl, M. Gallus, V. Welge, H. Esselmann, J. Wiltfang, Aminoterminally truncated and oxidized amyloid-beta peptides in the cerebrospinal fluid of Alzheimer's disease patients, J. Alzheimers Dis. 29 (2012) 809–816.
[15] N. Matsumura, M. Takami, M. Okochi, S. Wada-Kakuda, H. Fujiwara, S. Tagami, S. Funamoto, Y. Ihara, M. Morishima-Kawashima, Gamma-secretase associated with lipid rafts: multiple interactive pathways in the stepwise processing of beta-carboxyl-terminal fragment, J. Biol. Chem. 289 (2014) 5109–5121.
[16] M. Citron, T. Oltersdorf, C. Haass, L. McConlogue, A.Y. Hung, P. Seubert, C. Vigo-Pelfrey, I. Lieberburg, D.J. Selkoe, Mutation of the beta-amyloid precursor protein in familial Alzheimer's disease increases beta-protein production, Nature 360 (1992) 672–674.
[17] M. Citron, D. Westaway, W. Xia, G. Carlson, T. Diehl, G. Levesque, K. Johnson-Wood, M. Lee, P. Seubert, A. Davis, D. Kholodenko, R. Motter, R. Sherrington, B. Perry, H. Yao, R. Strome, I. Lieberburg, J. Rommens, S. Kim, D. Schenk, P. Fraser, P.S.G. Hyslop, D.J. Selkoe, Mutant presenilins of Alzheimer's disease increase production of 42-residue amyloid beta-protein in both transfected cells and transgenic mice, Nat. Med. 3 (1997) 67–72.
[18] D. Scheuner, C. Eckman, M. Jensen, X. Song, M. Citron, N. Suzuki, T.D. Bird, J. Hardy, M. Hutton, W. Kukull, E. Larson, E. Levy-Lahad, M. Viitanen, E. Peskind, P. Poorkaj, G. Schellenberg, R. Tanzi, W. Wasco, L. Lannfelt, D. Selkoe, S. Younkin, Secreted amyloid beta-protein similar to that in the senile plaques of Alzheimer's disease is increased in vivo by the presenilin 1 and 2 and APP mutations linked to familial Alzheimer's disease, Nat. Med. 2 (1996) 864–870.
[19] S. Kumar-Singh, J. Theuns, B. Van Broeck, D. Pirici, K. Vennekens, E. Corsmit, M. Cruts, B. Dermaut, R. Wang, C. Van Broeckhoven, Mean age-of-onset of familial Alzheimer disease caused by presenilin mutations correlates with both increased Abeta42 and decreased Abeta40, Hum. Mutat. 27 (2006) 686–695.
[20] M. Bentahir, O. Nyabi, J. Verhamme, A. Tolia, K. Horre, J. Wiltfang, H. Esselmann, B. De Strooper, Presenilin clinical mutations can affect gamma-secretase activity by different mechanisms, J. Neurochem. 96 (2006) 732–742.
[21] N. Suzuki, T.T. Cheung, X.D. Cai, A. Odaka, L. Otvos Jr., C. Eckman, T.E. Golde, S.G. Younkin, An increased percentage of long amyloid beta protein secreted by familial amyloid beta protein precursor (beta APP717) mutants, Science 264 (1994) 1336–1340.
[22] C. Haass, C.A. Lemere, A. Capell, M. Citron, P. Seubert, D. Schenk, L. Lannfelt, D.J. Selkoe, The Swedish mutation causes early-onset Alzheimer's disease by beta-secretase cleavage within the secretory pathway, Nat. Med. 1 (1995) 1291–1296.
[23] J. Hardy, D.J. Selkoe, The amyloid hypothesis of Alzheimer's disease: progress and problems on the road to therapeutics, Science 297 (2002) 353–356.
[24] J.A. Hardy, G.A. Higgins, Alzheimer's disease: the amyloid cascade hypothesis, Science 256 (1992) 184–185.
[25] L. Janssen, C. Keppens, P.P. De Deyn, D. Van Dam, Late age increase in soluble amyloid-beta levels in the APP23 mouse model despite steady-state levels of amyloid-beta-producing proteins, Biochim. Biophys. Acta 1862 (2016) 105–112.
[26] C. Sturchler-Pierrat, D. Abramowski, M. Duke, K.H. Wiederhold, C. Mistl, S. Rothacher, B. Ledermann, K. Burki, P. Frey, P.A. Paganetti, C. Waridel, M.E. Calhoun, M. Jucker, A. Probst, M. Staufenbiel, B. Sommer, Two amyloid precursor protein transgenic mouse models with Alzheimer disease-like pathology, Proc. Natl. Acad. Sci. U. S. A. 94 (1997) 13287–13292.
[27] C. Sturchler-Pierrat, M. Staufenbiel, Pathogenic mechanisms of Alzheimer's disease analyzed in the APP23 transgenic mouse model, Ann. N. Y. Acad. Sci. 920 (2000) 134–139.
[28] D. Van Dam, P. De Deyn, APP-based transgenic models: the APP23 model, in: P.P. De Deyn, D. Van Dam (Eds.), Animal Models of Dementia, Humana Press, Place Published 2011, pp. 399–413.
[29] B.W. Patterson, D.L. Elbert, K.G. Mawuenyega, T. Kasten, V. Ovod, S. Ma, C. Xiong, R. Chott, K. Yarasheski, W. Sigurdson, L. Zhang, A. Goate, T. Benzinger, J.C. Morris, D. Holtzman, R.J. Bateman, Age and amyloid effects on human CNS amyloid-beta kinetics, Ann. Neurol. (2015).
[30] R. Potter, B.W. Patterson, D.L. Elbert, V. Ovod, T. Kasten, W. Sigurdson, K. Mawuenyega, T. Blazey, A. Goate, R. Chott, K.E. Yarasheski, D.M. Holtzman, J.C. Morris, T.L. Benzinger, R.J. Bateman, Increased in vivo amyloid-beta42 production, exchange, and loss in presenilin mutation carriers, Sci. Transl. Med. 5 (2013) 189ra177.
[31] K.G. Mawuenyega, W. Sigurdson, V. Ovod, L. Munsell, T. Kasten, J.C. Morris, K.E. Yarasheski, R.J. Bateman, Decreased clearance of CNS beta-amyloid in Alzheimer's disease, Science 330 (2010) 1774.
[32] R.J. Bateman, L.Y. Munsell, J.C. Morris, R. Swarm, K.E. Yarasheski, D.M. Holtzman, Human amyloid-beta synthesis and clearance rates as measured in cerebrospinal fluid in vivo, Nat. Med. 12 (2006) 856–861.
[33] E. Hellstrom-Lindahl, R. Ravid, A. Nordberg, Age-dependent decline of neprilysin in Alzheimer's disease and normal brain: inverse correlation with A beta levels, Neurobiol. Aging 29 (2008) 210–221.
[34] B.T. Kress, J.J. Iliff, M. Xia, M. Wang, H.S. Wei, D. Zeppenfeld, L. Xie, H. Kang, Q. Xu, J.A. Liew, B.A. Plog, F. Ding, R. Deane, M. Nedergaard, Impairment of paravascular clearance pathways in the aging brain, Ann. Neurol. 76 (2014) 845–861.
[35] D.S. Yang, A. Kumar, P. Stavrides, J. Peterson, C.M. Peterhoff, M. Pawlik, E. Levy, A.M. Cataldo, R.A. Nixon, Neuronal apoptosis and autophagy cross talk in aging PS/APP mice, a model of Alzheimer's disease, Am. J. Pathol. 173 (2008) 665–681.
[36] A. Dobin, C.A. Davis, F. Schlesinger, J. Drenkow, C. Zaleski, S. Jha, P. Batut, M. Chaisson, T.R. Gingeras, STAR: ultrafast universal RNA-seq aligner, Bioinformatics 29 (2013) 15–21.
[37] S. Anders, P.T. Pyl, W. Huber, HTSeq–a Python framework to work with high-throughput sequencing data, Bioinformatics 31 (2015) 166–169.
[38] M.D. Robinson, D.J. McCarthy, G.K. Smyth, edgeR: a Bioconductor package for differential expression analysis of digital gene expression data, Bioinformatics 26 (2010) 139–140.
[39] P. Langfelder, S. Horvath, WGCNA: an R package for weighted correlation network analysis, BMC Bioinf. 9 (2008) 559.
[40] P. Langfelder, S. Horvath, Fast R functions for robust correlations and hierarchical clustering, J. Stat. Softw. 46 (2012).
[41] W. da Huang, B.T. Sherman, R.A. Lempicki, Systematic and integrative analysis of large gene lists using DAVID bioinformatics resources, Nat. Protoc. 4 (2009) 44–57.
[42] W. da Huang, B.T. Sherman, R.A. Lempicki, Bioinformatics enrichment tools: paths toward the comprehensive functional analysis of large gene lists, Nucleic Acids Res. 37 (2009) 1–13.
[43] J.A. Miller, C. Cai, P. Langfelder, D.H. Geschwind, S.M. Kurian, D.R. Salomon, S. Horvath, Strategies for aggregating gene expression data: the collapseRows R function, BMC Bioinf. 12 (2011) 322.
[44] I.J. Cajigas, G. Tushev, T.J. Will, S.t. Dieck, N. Fuerst, E.M. Schuman, The local transcriptome in the synaptic neuropil revealed by deep sequencing and high-resolution imaging, Neuron 74 (2012) 453–466.
[45] L. Bondolfi, M. Calhoun, F. Ermini, H.G. Kuhn, K.H. Wiederhold, L. Walker, M. Staufenbiel, M. Jucker, Amyloid-associated neuron loss and gliogenesis in the neocortex of amyloid precursor protein transgenic mice, J. Neurosci. 22 (2002) 515–522.
[46] M.E. Calhoun, K.H. Wiederhold, D. Abramowski, A.L. Phinney, A. Probst, C. Sturchler-Pierrat, M. Staufenbiel, B. Sommer, M. Jucker, Neuron loss in APP transgenic mice, Nature 395 (1998) 755–756.
[47] Y.T. Quiroz, A.P. Schultz, K. Chen, H.D. Protas, M. Brickhouse, A.S. Fleisher, J.B. Langbaum, P. Thiyyagura, A.M. Fagan, A.R. Shah, M. Muniz, J.F. Arboleda-Velasquez, C. Munoz, G. Garcia, N. Acosta-Baena, M. Giraldo, V. Tirado, D.L. Ramirez, P.N. Tariot, B.C. Dickerson, R.A. Sperling, F. Lopera, E.M. Reiman, Brain imaging and blood biomarker abnormalities in children with autosomal dominant Alzheimer disease: a cross-sectional study, JAMA Neurol. 72 (2015) 912–919.
[48] R. Sala-Llonch, A. Llado, J. Fortea, B. Bosch, A. Antonell, M. Balasa, N. Bargallo, D. Bartres-Faz, J.L. Molinuevo, R. Sanchez-Valle, Evolving brain structural changes in PSEN1 mutation carriers, Neurobiol. Aging 36 (2015) 1261–1270.
[49] Z. Wang, B. Wang, L. Yang, Q. Guo, N. Aithmitti, Z. Songyang, H. Zheng, Presynaptic and postsynaptic interaction of the amyloid precursor protein promotes peripheral and central synaptogenesis, J. Neurosci. 29 (2009) 10788–10801.
[50] M. Wines-Samuelson, J. Shen, Presenilins in the developing, adult, and aging cerebral cortex, Neuroscientist 11 (2005) 441–451.
[51] M. Klevanski, U. Herrmann, S.W. Weyer, R. Fol, N. Cartier, D.P. Wolfer, J.H. Caldwell, M. Korte, U.C. Muller, The APP intracellular domain is required for normal synaptic morphology, synaptic plasticity, and hippocampus-dependent behavior, J. Neurosci. 35 (2015) 16018–16033.

[52] P. Song, S.W. Pimplikar, Knockdown of amyloid precursor protein in zebrafish causes defects in motor axon outgrowth, PLoS One 7 (2012), e34209.
[53] D. Van Dam, R. D'Hooge, M. Staufenbiel, C. Van Ginneken, F. Van Meir, P.P. De Deyn, Age-dependent cognitive decline in the APP23 model precedes amyloid deposition, Eur. J. Neurosci. 17 (2003) 388–396.
[54] E. Vloeberghs, D. Van Dam, R. D'Hooge, M. Staufenbiel, P.P. De Deyn, APP23 mice display working memory impairment in the plus-shaped water maze, Neurosci. Lett. 407 (2006) 6–10.
[55] L. Prut, D. Abramowski, T. Krucker, C.L. Levy, A.J. Roberts, M. Staufenbiel, C. Wiessner, Aged APP23 mice show a delay in switching to the use of a strategy in the Barnes maze, Behav. Brain Res. 179 (2007) 107–110.
[56] R. Lalonde, M. Dumont, M. Staufenbiel, C. Sturchler-Pierrat, C. Strazielle, Spatial learning, exploration, anxiety, and motor coordination in female APP23 transgenic mice with the Swedish mutation, Brain Res. 956 (2002) 36–44.
[57] P.H. Kelly, L. Bondolfi, D. Hunziker, H.P. Schlecht, K. Carver, E. Maguire, D. Abramowski, K.H. Wiederhold, C. Sturchler-Pierrat, M. Jucker, R. Bergmann, M. Staufenbiel, B. Sommer, Progressive age-related impairment of cognitive behavior in APP23 transgenic mice, Neurobiol. Aging 24 (2003) 365–378.
[58] R. Hellweg, P. Lohmann, R. Huber, A. Kuhl, M.W. Riepe, Spatial navigation in complex and radial mazes in APP23 animals and neurotrophin signaling as a biological marker of early impairment, Learn. Mem. 13 (2006) 63–71.
[59] M. Dumont, C. Strazielle, M. Staufenbiel, R. Lalonde, Spatial learning and exploration of environmental stimuli in 24-month-old female APP23 transgenic mice with the Swedish mutation, Brain Res. 1024 (2004) 113–121.
[60] K.D. Bornemann, M. Staufenbiel, Transgenic mouse models of Alzheimer's disease, Ann. N. Y. Acad. Sci. 908 (2000) 260–266.
[61] K.D. Bornemann, K.H. Wiederhold, C. Pauli, F. Ermini, M. Stalder, L. Schnell, B. Sommer, M. Jucker, M. Staufenbiel, Abeta-induced inflammatory processes in microglia cells of APP23 transgenic mice, Am. J. Pathol. 158 (2001) 63–73.
[62] A.L. Phinney, T. Deller, M. Stalder, M.E. Calhoun, M. Frotscher, B. Sommer, M. Staufenbiel, M. Jucker, Cerebral amyloid induces aberrant axonal sprouting and ectopic terminal formation in amyloid precursor protein transgenic mice, J. Neurosci. 19 (1999) 8552–8559.
[63] M. Stalder, A. Phinney, A. Probst, B. Sommer, M. Staufenbiel, M. Jucker, Association of microglia with amyloid plaques in brains of APP23 transgenic mice, Am. J. Pathol. 154 (1999) 1673–1684.
[64] L.F. Maia, S.A. Kaeser, J. Reichwald, M. Lambert, U. Obermuller, J. Schelle, J. Odenthal, P. Martus, M. Staufenbiel, M. Jucker, Increased CSF Abeta during the very early phase of cerebral Abeta deposition in mouse models, EMBO Mol. Med. (2015).
[65] R.A. Sperling, P.S. Aisen, L.A. Beckett, D.A. Bennett, S. Craft, A.M. Fagan, T. Iwatsubo, C.R. Jack Jr., J. Kaye, T.J. Montine, D.C. Park, E.M. Reiman, C.C. Rowe, E. Siemers, Y. Stern, K. Yaffe, M.C. Carrillo, B. Thies, M. Morrison-Bogorad, M.V. Wagster, C.H. Phelps, Toward defining the preclinical stages of Alzheimer's disease: recommendations from the National Institute on Aging-Alzheimer's Association workgroups on diagnostic guidelines for Alzheimer's disease, Alzheimers Dement. 7 (2011) 280–292.
[66] K. Flurkey, J.M. Currer, D.E. Harrison, Chapter 20 — Mouse models in aging research A2, in: J.G. Fox, M.T. Davisson, F.W. Quimby, S.W. Barthold, C.E. Newcomer, A.L. Smith (Eds.), The Mouse in Biomedical Research, second ed.Academic Press, Place Published 2007, pp. 637–672.
[67] D. Van Dam, B. Marescau, S. Engelborghs, T. Cremers, J. Mulder, M. Staufenbiel, P.P. De Deyn, Analysis of cholinergic markers, biogenic amines, and amino acids in the CNS of two APP overexpression mouse models, Neurochem. Int. 46 (2005) 409–422.
[68] S. Boncristiano, M.E. Calhoun, P.H. Kelly, M. Pfeifer, L. Bondolfi, M. Stalder, A.L. Phinney, D. Abramowski, C. Sturchler-Pierrat, A. Enz, B. Sommer, M. Staufenbiel, M. Jucker, Cholinergic changes in the APP23 transgenic mouse model of cerebral amyloidosis, J. Neurosci. 22 (2002) 3234–3243.
[69] M.E. Calhoun, P. Burgermeister, A.L. Phinney, M. Stalder, M. Tolnay, K.H. Wiederhold, D. Abramowski, C. Sturchler-Pierrat, B. Sommer, M. Staufenbiel, M. Jucker, Neuronal overexpression of mutant amyloid precursor protein results in prominent deposition of cerebrovascular amyloid, Proc. Natl. Acad. Sci. U. S. A. 96 (1999) 14088–14093.
[70] D.T. Winkler, L. Bondolfi, M.C. Herzig, L. Jann, M.E. Calhoun, K.H. Wiederhold, M. Tolnay, M. Staufenbiel, M. Jucker, Spontaneous hemorrhagic stroke in a mouse model of cerebral amyloid angiopathy, J. Neurosci. 21 (2001) 1619–1627.
[71] S. Roder, L. Danober, M.F. Pozza, K. Lingenhoehl, K.H. Wiederhold, H.R. Olpe, Electrophysiological studies on the hippocampus and prefrontal cortex assessing the effects of amyloidosis in amyloid precursor protein 23 transgenic mice, Neuroscience 120 (2003) 705–720.
[72] E. Vloeberghs, D. Van Dam, S. Engelborghs, G. Nagels, M. Staufenbiel, P.P. De Deyn, Altered circadian locomotor activity in APP23 mice: a model for BPSD disturbances, Eur. J. Neurosci. 20 (2004) 2757–2766.
[73] E. Vloeberghs, D. Van Dam, K. Coen, M. Staufenbiel, P.P. De Deyn, Aggressive male APP23 mice modeling behavioral alterations in dementia, Behav. Neurosci. 120 (2006) 1380–1383.
[74] I.R. Holtman, D.D. Raj, J.A. Miller, W. Schaafsma, Z. Yin, N. Brouwer, P.D. Wes, T. Moller, M. Orre, W. Kamphuis, E.M. Hol, E.W. Boddeke, B.J. Eggen, Induction of a common microglia gene expression signature by aging and neurodegenerative conditions: a co-expression meta-analysis, Acta Neuropathol. Commun. 3 (2015) 31.
[75] Z. Yin, D. Raj, N. Saiepour, D. Van Dam, N. Brouwer, B.J.L. Eggen, U.K. Hanisch, E.M. Hol, W.A. Kamphuis, T.A. Bayer, P.P. De deyn, H.W.G.W. Boddeke, Beta-amyloid plaque associated microglia priming in Alzheimer's disease, Sci. Immunol. (2016) (under submission).
[76] D. Avramopoulos, M. Szymanski, R. Wang, S. Bassett, Gene expression reveals overlap between normal aging and Alzheimer's disease genes, Neurobiol. Aging 32 (2011) 2319.e27–2319.e34.
[77] K. Bossers, K.T. Wirz, G.F. Meerhoff, A.H. Essing, J.W. van Dongen, P. Houba, C.G. Kruse, J. Verhaagen, D.F. Swaab, Concerted changes in transcripts in the prefrontal cortex precede neuropathology in Alzheimer's disease, Brain J. Neurol. 133 (2010) 3699–3723.
[78] M. Orre, W. Kamphuis, L.M. Osborn, A.H. Jansen, L. Kooijman, K. Bossers, E.M. Hol, Isolation of glia from Alzheimer's mice reveals inflammation and dysfunction, Neurobiol. Aging 35 (2014) 2746–2760.
[79] K.T. Wirz, K. Bossers, A. Stargardt, W. Kamphuis, D.F. Swaab, E.M. Hol, J. Verhaagen, Cortical beta amyloid protein triggers an immune response, but no synaptic changes in the APPswe/PS1dE9 Alzheimer's disease mouse model, Neurobiol. Aging 34 (2013) 1328–1342.
[80] B. Zhang, C. Gaiteri, L.G. Bodea, Z. Wang, J. McElwee, A.A. Podtelezhnikov, C. Zhang, T. Xie, L. Tran, R. Dobrin, E. Fluder, B. Clurman, S. Melquist, M. Narayanan, C. Suver, H. Shah, M. Mahajan, T. Gillis, J. Mysore, M.E. MacDonald, J.R. Lamb, D.A. Bennett, C. Molony, D.J. Stone, V. Gudnason, A.J. Myers, E.E. Schadt, H. Neumann, J. Zhu, V. Emilsson, Integrated systems approach identifies genetic nodes and networks in late-onset Alzheimer's disease, Cell 153 (2013) 707–720.
[81] X.K. Wang, M.L. Michaelis, E.K. Michaelis, Functional genomics of brain aging and Alzheimer's disease: focus on selective neuronal vulnerability, Curr. Genomics 11 (2010) 618–633.
[82] C. Franceschi, M. Bonafe, S. Valensin, F. Olivieri, M. De Luca, E. Ottaviani, G. De Benedictis, Inflamm-aging. An evolutionary perspective on immunosenescence, Ann. N. Y. Acad. Sci. 908 (2000) 244–254.
[83] C. Franceschi, M. Capri, D. Monti, S. Giunta, F. Olivieri, F. Sevini, M.P. Panourgia, L. Invidia, L. Celani, M. Scurti, E. Cevenini, G.C. Castellani, S. Salvioli, Inflammaging and anti-inflammaging: a systemic perspective on aging and longevity emerged from studies in humans, Mech. Ageing Dev. 128 (2007) 92–105.
[84] E. Montecino-Rodriguez, B. Berent-Maoz, K. Dorshkind, Causes, consequences, and reversal of immune system aging, J. Clin. Invest. 123 (2013) 958–965.
[85] M. Malik, I. Parikh, J.B. Vasquez, C. Smith, L. Tai, G. Bu, M.J. LaDu, D.W. Fardo, G.W. Rebeck, S. Estus, Genetics ignite focus on microglial inflammation in Alzheimer's disease, Mol. Neurodegener. 10 (2015) 52.
[86] W.J. Streit, H. Braak, Q.S. Xue, I. Bechmann, Dystrophic (senescent) rather than activated microglial cells are associated with tau pathology and likely precede neurodegeneration in Alzheimer's disease, Acta Neuropathol. 118 (2009) 475–485.
[87] W.J. Streit, N.W. Sammons, A.J. Kuhns, D.L. Sparks, Dystrophic microglia in the aging human brain, Glia 45 (2004) 208–212.
[88] A. Griciuc, A. Serrano-Pozo, A.R. Parrado, A.N. Lesinski, C.N. Asselin, K. Mullin, B. Hooli, S.H. Choi, B.T. Hyman, R.E. Tanzi, Alzheimer's disease risk gene CD33 inhibits microglial uptake of amyloid beta, Neuron 78 (2013) 631–643.
[89] S. Hellwig, A. Masuch, S. Nestel, N. Katzmarski, M. Meyer-Luehmann, K. Biber, Forebrain microglia from wild-type but not adult 5xFAD mice prevent amyloid-beta plaque formation in organotypic hippocampal slice cultures, Sci. Rep. 5 (2015) 14624.
[90] G. Krabbe, A. Halle, V. Matyash, J.L. Rinnenthal, G.D. Eom, U. Bernhardt, K.R. Miller, S. Prokop, H. Kettenmann, F.L. Heppner, Functional impairment of microglia coincides with Beta-amyloid deposition in mice with Alzheimer-like pathology, PLoS One 8 (2013), e60921.
[91] S. Mueller-Steiner, Y. Zhou, H. Arai, E.D. Roberson, B. Sun, J. Chen, X. Wang, G. Yu, L. Esposito, L. Mucke, L. Gan, Antiamyloidogenic and neuroprotective functions of cathepsin B: implications for Alzheimer's disease, Neuron 51 (2006) 703–714.
[92] B. Sun, Y. Zhou, B. Halabisky, I. Lo, S.H. Cho, S. Mueller-Steiner, N. Devidze, X. Wang, A. Grubb, L. Gan, Cystatin C-cathepsin B axis regulates amyloid beta levels and associated neuronal deficits in an animal model of Alzheimer's disease, Neuron 60 (2008) 247–257.
[93] C. Wang, B. Sun, Y. Zhou, A. Grubb, L. Gan, Cathepsin B degrades amyloid-beta in mice expressing wild-type human amyloid precursor protein, J. Biol. Chem. 287 (2012) 39834–39841.
[94] J.S. Miners, N. Barua, P.G. Kehoe, S. Gill, S. Love, Abeta-degrading enzymes: potential for treatment of Alzheimer disease, J. Neuropathol. Exp. Neurol. 70 (2011) 944–959.
[95] H.J. Carlisle, M.B. Kennedy, Spine architecture and synaptic plasticity, Trends Neurosci. 28 (2005) 182–187.
[96] V. Schubert, C.G. Dotti, Transmitting on actin: synaptic control of dendritic architecture, J. Cell Sci. 120 (2007) 205–212.
[97] Y. Sekino, N. Kojima, T. Shirao, Role of actin cytoskeleton in dendritic spine morphogenesis, Neurochem. Int. 51 (2007) 92–104.
[98] A.K. Fu, K.W. Hung, H. Huang, S. Gu, Y. Shen, E.Y. Cheng, F.C. Ip, X. Huang, W.Y. Fu, N.Y. Ip, Blockade of EphA4 signaling ameliorates hippocampal synaptic dysfunctions in mouse models of Alzheimer's disease, Proc. Natl. Acad. Sci. U. S. A. 111 (2014) 9959–9964.
[99] L.M. Vargas, N. Leal, L.D. Estrada, A. Gonzalez, F. Serrano, K. Araya, K. Gysling, N.C. Inestrosa, E.B. Pasquale, A.R. Alvarez, EphA4 activation of c-Abl mediates synaptic loss and LTP blockade caused by amyloid-beta oligomers, PLoS One 9 (2014), e92309.
[100] M. Cisse, B. Halabisky, J. Harris, N. Devidze, D.B. Dubal, B. Sun, A. Orr, G. Lotz, D.H. Kim, P. Hamto, K. Ho, G.Q. Yu, L. Mucke, Reversing EphB2 depletion rescues cognitive functions in Alzheimer model, Nature 469 (2011) 47–52.
[101] M.H. Magdesian, M. Gralle, L.H. Guerreiro, P.J. Beltrao, M.M. Carvalho, L.E. Santos, F.G. de Mello, R.A. Reis, S.T. Ferreira, Secreted human amyloid precursor protein binds semaphorin 3a and prevents semaphorin-induced growth cone collapse, PLoS One 6 (2011), e22857.
[102] Q.L. Ma, F. Yang, F. Calon, O.J. Ubeda, J.E. Hansen, R.H. Weisbart, W. Beech, S.A. Frautschy, G.M. Cole, p21-activated kinase-aberrant activation and

translocation in Alzheimer disease pathogenesis, J. Biol. Chem. 283 (2008) 14132–14143.
[103] A. Mendoza-Naranjo, E. Contreras-Vallejos, D.R. Henriquez, C. Otth, J.R. Bamburg, R.B. Maccioni, C. Gonzalez-Billault, Fibrillar amyloid-beta1-42 modifies actin organization affecting the cofilin phosphorylation state: a role for Rac1/cdc42 effector proteins and the slingshot phosphatase, J. Alzheimers Dis. 29 (2012) 63–77.
[104] L. Zhao, Q.L. Ma, F. Calon, M.E. Harris-White, F. Yang, G.P. Lim, T. Morihara, O.J. Ubeda, S. Ambegaokar, J.E. Hansen, R.H. Weisbart, B. Teter, S.A. Frautschy, G.M. Cole, Role of p21-activated kinase pathway defects in the cognitive deficits of Alzheimer disease, Nat. Neurosci. 9 (2006) 234–242.
[105] K.S. Shim, G. Lubec, Drebrin, a dendritic spine protein, is manifold decreased in brains of patients with Alzheimer's disease and Down syndrome, Neurosci. Lett. 324 (2002) 209–212.
[106] K. Hatanpaa, K.R. Isaacs, T. Shirao, D.R. Brady, S.I. Rapoport, Loss of proteins regulating synaptic plasticity in normal aging of the human brain and in Alzheimer disease, J. Neuropathol. Exp. Neurol. 58 (1999) 637–643.
[107] H. Takahashi, Y. Sekino, S. Tanaka, T. Mizui, S. Kishi, T. Shirao, Drebrin-dependent actin clustering in dendritic filopodia governs synaptic targeting of postsynaptic density-95 and dendritic spine morphogenesis, J. Neurosci. 23 (2003) 6586–6595.
[108] R.C. May, L.M. Machesky, Phagocytosis and the actin cytoskeleton, J. Cell Sci. 114 (2001) 1061–1077.
[109] J.D. Cahoy, B. Emery, A. Kaushal, L.C. Foo, J.L. Zamanian, K.S. Christopherson, Y. Xing, J.L. Lubischer, P.A. Krieg, S.A. Krupenko, W.J. Thompson, B.A. Barres, A transcriptome database for astrocytes, neurons, and oligodendrocytes: a new resource for understanding brain development and function, 2008. J. Neurosci. 28 (1) 264–278, http://dx.doi.org/10.1523/JNEUROSCI.4178-07.2008.